Evolution of anti–de Sitter black holes in Einstein-Maxwell-dilaton theory

Cheng-Yong Zhang,[1,*] Peng Liu,[1,†] Yunqi Liu,[2,‡] Chao Niu,[1,§] and Bin Wang[2,3,‖]

[1]*Department of Physics and Siyuan Laboratory, Jinan University, Guangzhou 510632, China*
[2]*Center for Gravitation and Cosmology, College of Physical Science and Technology, Yangzhou University, Yangzhou 225009, China*
[3]*School of Aeronautics and Astronautics, Shanghai Jiao Tong University, Shanghai 200240, China*

(Received 4 July 2021; accepted 7 December 2021; published 4 January 2022)

We study the nonlinear evolution of the spherical symmetric charged black holes under a small neutral scalar field perturbation in Einstein-Maxwell-dilaton theory with coupling function $f(\phi) = e^{-b\phi}$ in asymptotic anti–de Sitter spacetime. The nonminimal coupling between scalar and Maxwell fields allows the transmission of the energy from the Maxwell field to the scalar field, but also behaves as a repulsive force for the scalar. The scalar field oscillates with damping amplitude and converges to a final value. The irreducible mass of the black hole increases abruptly at initial times and then saturates to the final value exponentially. The saturating rate is twice the decaying rate of the dominant mode of the scalar. The effects of the black hole charge, the cosmological constant, and the coupling parameter on the evolution are studied in detail. When the initial configuration is a naked singularity spacetime with a large charge to mass ratio, a horizon will form soon and hide the singularity.

DOI: 10.1103/PhysRevD.105.024010

I. INTRODUCTION

The famous no-hair theorem in Einstein-Maxwell theory and its generalization in scalar-tensor theory shows that a black hole can be completely characterized by 3 degrees of freedom: its mass, charge, and angular momentum [1–7]. However, there are exceptions to the rule as well. In gravitational theories beyond general relativity (GR) the dilatonic and colored black holes in the Einstein-dilaton-Gauss-Bonnet theory [8,9] and the rotating [10–12] or higher-dimensional [13–18] or shift-symmetric Galileon [19–21] hairy black hole solutions circumvent the no-hair theorem. Even GR with certain matter sources could evade the no-hair theorem, such as black hole solutions with a Yang-Mills field [22–25], Skyrme field [26,27], and a conformally coupled scalar field [28]. Recently, as a dynamic mechanism leading to hairy black hole solutions under the frame of GR, spontaneous scalarization has attracted much attention. It was initially proposed in the study of the neutron star and also happens when black holes are surrounded by enough matter in scalar-tensor theory [29–33]. Recent studies show that spontaneous scalarization could exist typically in the models containing nonminimal coupling of a real scalar field to the source terms which could be either the geometric invariant sources such as the Ricci scalar, Gauss-Bonnet, Chern-Simons invariant [34–46], or the matter invariant sources such as the Maxwell invariant in Einstein-Maxwell-scalar (EMS) theory [47–53] and the Einstein-Maxwell-vector model [54]. The successful observation of gravitational waves [55,56] and the black hole shadow [57–59] have pushed the research and theoretical detection of black holes into a new era providing a new window to test the characteristics of black holes. Thus it is necessary to carefully study the physics on hairy black holes such as metrics, the dynamic process of formation and evolution, and use the observation to test no-hair theorem or constraint the families of black holes [60,61].

As a natural and simple generalization of the Einstein-Maxwell theory, the Einstein-Maxwell-dilaton (EMD) theory occurs in the context of Kaluza-Klein theories in which the scalar field describes how the extra dimensions dilate along the four-dimensional spacetime [62] It also originates from the low-energy limit of string theory and is ubiquitous in supergravity [63]. The dilaton couples to the Maxwell term nonminimally and prevents the Reissner-Nordström (RN) solution in EMD theory. Instead, only dilatonic black hole solutions exist that present some RN-unlike features such as that the black hole charge to mass ratio can exceed unity [64–66]. The solutions here have mass, charge, rotation, and scalar hair, together with scalar, vector, and tensor radiative channels, and therefore offer an interesting theoretical and computational playground to explore possible deviations from the general relativity prediction.

*zhangcy@email.jnu.edu.cn
†Corresponding author.
phylp@email.jnu.edu.cn
‡yunqiliu@yzu.edu.cn
§niuchaophy@gmail.com
‖wang_b@sjtu.edu.cn

The mathematical structure of the EMD model allows for defining a well posed initial value problem rather than those in the extended scalar-tensor-Gauss-Bonnet models [67–72]. In asymptotic flat spacetime for EMD theory, the black hole endowed with a potential emerging from low-energy heterotic string theory was found nonlinearly stable under perturbations [73]. The dynamical evolution of individual black holes, as well as the merger of binary black hole systems, was analyzed in [74]. Hirschmann *et al.* found that the black hole systems are difficult to distinguish from their analogs within general relativity when the charge is relatively small. The dynamics in EMS models with more generic nonminimally coupling functions are also of interest, especially from the viewpoint of spontaneous scalarization. Here the RN black hole is a solution but unstable against scalar perturbations for a sufficiently large charge to mass ratio. The scalar hairy black hole solution is energetically and dynamically favored [47,53,75].

In this paper, we will study the evolution of spherically symmetric charged black holes in anti–de Sitter (AdS) spacetime in EMD theory. It is known that the cosmological constant can significantly affect the scalarization of the black hole [32]. The regular hairy black hole solutions exist in all asymptotic flat, de Sitter (dS), and AdS spacetime in EMS models [48,76,77]. While in the extended scalar-tensor-Gauss-Bonnet model, they exist only in asymptotic flat and AdS spacetime [78]. The positive cosmological constant can quench the tachyonic instability. While the dynamically and thermodynamically stable scalarized black holes can exist in EMD theory [73]. Therefore, it is necessary to study the full nonlinear dynamical evolution of the black holes in asymptotic AdS spacetime in EMD theory and compare the results with those in asymptotic flat spacetime. Note that the dynamics in AdS spacetime is qualitatively different from those in asymptotic flat spacetime since the scalar modes can propagate to the spacial boundary in finite coordinate time and be bounced back. The studies in asymptotic AdS spacetime cannot be naively generalized to the case of asymptotically flat spacetime since their boundary behaviors are distinct.

This paper is organized as follows. In Sec. II, we introduce the equations of motions and boundary behaviors of the variables in EMD theory. In Sec. III, we demonstrate the numerical results, where the effects of the coupling function parameter b (III A), the charge (III B), and the cosmological constant (III C) on the dynamical scalarization are studied in detail. Section IV gives the summary and discussion.

II. EINSTEIN-MAXWELL-DILATON THEORY

The action of Einstein-Maxwell-dilaton theory in AdS spacetime in this work is

$$S=\frac{1}{16\pi}\int d^4x\sqrt{-g}[R-2\Lambda-2\nabla_\mu\phi\nabla^\mu\phi-e^{-b\phi}F_{\mu\nu}F^{\mu\nu}]. \tag{1}$$

The cosmological constant Λ is negative for asymptotic AdS spacetime. R is the Ricci scalar of the metric $g_{\mu\nu}$. The Maxwell field strength is $F_{\mu\nu}=\partial_\mu A_\nu-\partial_\nu A_\mu$ in which A_μ is the gauge field. The coupling function between the real dilaton ϕ and gauge field is $f(\phi)=e^{-b\phi}$ in which the parameter b is a constant. Note that the action is invariant under the $\mathbb{Z}_2$ symmetry $(b,\phi)\to-(b,\phi)$. Hereafter, we keep $-b>0$ in this paper without loss of generality. The dilatonic coupling function appears in Kaluza-Klein models, supergravity, or low-energy string models. Some of the exact solutions in asymptotic flat spacetime are obtained in [64,65].

The equations of motion are

$$R_{\mu\nu}-\frac{1}{2}Rg_{\mu\nu}+\Lambda g_{\mu\nu}=2\left[\partial_\mu\phi\partial_\nu\phi-\frac{1}{2}g_{\mu\nu}\nabla_\rho\phi\nabla^\rho\phi+e^{-b\phi}\left(F_{\mu\rho}F_\nu{}^\rho-\frac{1}{4}g_{\mu\nu}F_{\rho\sigma}F^{\rho\sigma}\right)\right], \tag{2}$$

$$\nabla_\mu\nabla^\mu\phi=-\frac{b}{4}e^{-b\phi}F_{\mu\nu}F^{\mu\nu}, \tag{3}$$

$$\nabla_\mu(f(\phi)F^{\mu\nu})=0. \tag{4}$$

It is obvious that $\phi=0$ will not be a solution of Eq. (3) unless $A_\mu=0$ and thus the RN-AdS black hole is not a solution of EMD theory. However, when ϕ is very small, one could obtain a solution that is very close to the RN-AdS black hole. This solution is unstable and a stable black hole with nontrivial scalar hair will form at the end. Our numerical simulation studies this nonlinear dynamic process in detail. To implement the simulation, we take the ingoing Eddington-Finkelstein coordinate ansatz

$$ds^2=-\alpha(t,r)dt^2+2dtdr+\zeta(t,r)^2(d\theta^2+\sin^2\theta d\phi^2). \tag{5}$$

The coordinate is regular on the black hole apparent horizon which is defined by

$$0=g^{ab}\partial_a\zeta\partial_b\zeta. \tag{6}$$

Here indices $a,b\in\{t,r\}$. Once we get the apparent horizon r_a, we can get the irreducible mass of the black hole $M_0=\sqrt{\frac{A}{4\pi}}=\zeta(t,r_a)$ in which $A=4\pi\zeta^2(t,r_a)$ is the area of the black hole. As the black hole area does not decrease, we will see that the irreducible mass of the black hole will not decrease in the evolution. On the other hand, we will study the rescaled Misner-Sharp mass defined as

$M_{\rm MS} = \frac{m}{4\pi}$ in which the generalized Misner-Sharp quasi-local mass is defined by [79]

$$m = 2\pi\zeta\left(-\frac{\Lambda}{3}\zeta^2 + 1 - g^{ab}\partial_a\zeta\partial_b\zeta\right). \tag{7}$$

The rescaled Misner-Sharp mass tends to the ADM mass of the spacetime as $r \to \infty$.

We also require the gauge potential $A_\mu dx^\mu = A(t,r)dt$ and the dilaton $\phi = \phi(t,r)$. With these choices, the Maxwell field can be worked out as

$$\partial_r A = \frac{Q}{\zeta^2 f(\phi)}, \tag{8}$$

in which Q is a constant interpreted as the electric charge of the black hole. Equation (8) indicates the strength of the Maxwell field. The coupling function $f(\phi)$ acts as an effective dielectric that varies the strength. To implement the numerics, we introduce auxiliary variables

$$S = \partial_t\zeta + \frac{1}{2}\alpha\partial_r\zeta, \qquad P = \partial_t\phi + \frac{1}{2}\alpha\partial_r\phi. \tag{9}$$

Then the Einstein equations become

$$\partial_t S = \frac{1}{2}S\partial_r\alpha + \frac{\alpha}{2}\left(\frac{2S\partial_r\zeta - 1}{2\zeta} + \frac{1}{2}\zeta\Lambda + \frac{Q^2}{2\zeta^3 f(\phi)}\right) - \zeta P^2, \tag{10}$$

$$\partial_r^2\alpha = -4P\partial_r\phi + \frac{4S\partial_r\zeta - 2}{\zeta^2} + \frac{4Q^2}{\zeta^4 f(\phi)}, \tag{11}$$

$$\partial_r S = \frac{1 - 2S\partial_r\zeta}{2\zeta} - \frac{\zeta\Lambda}{2} - \frac{Q^2}{2\zeta^3 f(\phi)}, \tag{12}$$

$$\partial_r^2\zeta = -\zeta(\partial_r\phi)^2. \tag{13}$$

The scalar equation becomes

$$P' = -\frac{P\zeta' + S\phi'}{\zeta} - \frac{Q^2}{4\zeta^4 f(\phi)^2}\frac{df(\phi)}{d\phi}. \tag{14}$$

Given an initial ϕ, we can integrate Eqs. (11), (12), (13), and (14) to get α, S, ζ, P at the initial time. Then from Eq. (9) we get the ϕ at the next time step. Equation (10) is redundant and can be used to check the accuracy of the numerical code. To solve these equations numerically, we need to specify boundary conditions. Expanding the variables in the asymptotic infinity, we get the asymptotic solutions

$$\phi = \frac{\phi_3(t)}{r^3} + \frac{3}{8\Lambda r^4}(-bQ^2 - 8\phi_3'(t)) + O(r^{-5}), \tag{15}$$

$$\alpha = -\frac{\Lambda}{3}r^2 + 1 - \frac{2M}{r} + \frac{Q^2}{r^2} + \frac{\Lambda}{5r^4}\phi_3^2(t) + O(r^{-5}), \tag{16}$$

$$\zeta = r - \frac{3\phi_3^2(t)}{10r^5} + \frac{3\phi_3(t)}{14\Lambda r^6}(-bQ^2 - 8\phi_3'(t)) + O(r^{-7}), \tag{17}$$

$$S = -\frac{\Lambda}{6}r^2 + \frac{1}{2} - \frac{M}{r} + \frac{Q^2}{2r^2} - \frac{3\Lambda}{20r^4}\phi_3^2(t) + O(r^{-5}), \tag{18}$$

$$P = \frac{\Lambda\phi_3(t)}{2r^2} + \frac{1}{r^3}\left(\frac{-bQ^2}{4} - \phi_3'(t)\right) + \frac{3}{2\Lambda r^4}\phi_3''(t) + O(r^{-5}), \tag{19}$$

in which $\phi_3'(t) = \frac{d\phi_3(t)}{dt}$. The free parameters of the asymptotic solution are the Arnowitt-Deser-Misner (ADM) mass M and charge Q of the black hole, and the cosmological constant Λ. Function $\phi_3(t)$ is unknown and should be determined by evolution. In the static case, ϕ_3 can be viewed as the parameter indicating the existence of the scalar hair. Note that we have set $\zeta - r = 0$ as $r \to \infty$ by fixing the residual radial reparametrization freedom [80]. Some variables such as ζ, α, and S are divergent at infinity. We introduce the following new variables to do the numerical calculation:

$$\zeta \equiv r\sigma, \qquad \alpha \equiv r^2 a, \qquad S \equiv r^2 s, \qquad P \equiv \frac{1}{r}p. \tag{20}$$

In asymptotic AdS spacetime, the scalar perturbation can reach the infinity in finite coordinate time and be bounced back to the bulk. We must include the infinity in the computational domain. We thus compactify the radial direction by a coordinate transformation:

$$z = \frac{r}{r + M}. \tag{21}$$

The computation domain in the z coordinate is then $(z_0, 1)$ where z_0 corresponds to some radius r_0 which is close to the black hole horizon from inside and $z = 1$ corresponds to radial infinity. Now the boundary conditions at $z = 1$ are

$$\sigma = 1, \qquad \sigma' = 0, \qquad s = -\frac{\Lambda}{6}, \qquad s' = 0, \qquad s'' = 6(M-1), \tag{22}$$

$$p = 0, \qquad a = -\frac{\Lambda}{3}, \qquad a' = 0, \qquad a'' = 12(M-1). \tag{23}$$

The z direction is uniformly discretized. Equations (11), (13), and (14) are discretized with a fourth-order finite difference while Eq. (12) is discretized with a second-order finite difference. The time direction marches with fourth-order Runge-Kutta method. We employ Kreiss-Oliger dissipation to stabilize the numerical evolution.

III. NUMERICAL RESULTS

The free parameter of the system is the black hole charge Q, ADM mass M, and the cosmological constant Λ. We take the initial dilaton profile as

$$\phi_0 = \kappa e^{-\frac{(r-4r_h)^2}{w^2}} \quad \text{or}$$
$$\phi_0 = \begin{cases} (\frac{1}{r}-\frac{1}{r_1})^3(\frac{1}{r}-\frac{1}{r_2})^3 \frac{\kappa_1+\kappa_2 \sin\frac{10}{r}}{r^2}, & r_1 < r < r_2, \\ 0, & r \le r_1 \text{ or } r \ge r_2. \end{cases} \tag{24}$$

Here, $\kappa < 10^{-9}$ and width $w = 1.8r_h$ where r_h is the horizon radius of the initial black hole. Initial parameters $\{r_1, r_2\} = \{2r_h, 3r_h\}$, and κ_1, κ_2 are of order 10^{-2} so that the initial scalar field is of order 10^{-10} and negligible compared to the initial black hole. Hereafter, we fix $M = 1$ in this paper to implement the dimension-lessness of the physical quantities.

We show the sketches of the very early time evolutions of metric α and scalar ϕ in Fig. 1. For small $-\Lambda$, the extremal charge of the initial extremal black hole is about $Q_e \simeq M = 1$. When $Q < Q_e$, the initial configuration is a black hole spacetime. Part of the energy of the Maxwell field is transferred to the scalar field due to their non-minimal coupling. The scalar field grows rapidly and is captured by the black hole. So the scalar decreases monotonically in the radial direction and the radius of the apparent horizon increases with time.

When $Q > Q_e$, the initial solution we could obtain is a spacetime with naked singularity. Surprisingly, we find that our numerical codes work well with the initial condition $\phi_0 = \kappa \exp^{-\frac{(r-4M)^2}{(1.8M)^2}}$ when Q is greater than Q_e but not too large. As shown in the right panels of Fig. 1, the initial configuration is a spacetime with naked singularity. But a horizon forms soon and hides the singularity, resulting in a regular spacetime geometry outside the horizon. In fact, since there is no well-defined initial value problem for the naked singularity, we cannot do the simulation straightforwardly for the whole space region. Instead, we only evolve the region ranging from a cutoff r_0 to the infinity. Due to the divergence near the central singularity, the cutoff cannot be too small. In fact, from the metric ansatz we know that the light signal propagates with $\frac{dr}{dt} = \frac{\alpha}{2}$. In Fig. 1, the cutoff locates at $r_0 \simeq 0.8$ and the initial metric function at r_0 is $\alpha(r_0) \simeq 0.6$. It takes $\Delta t \simeq 0.04$ when the apparent horizon forms (see the sixth line from the top for example in the upper right panel of Fig. 1). So the influence region of the initial information at the cutoff is at most $r_0 + \Delta r \le r_0 + \frac{\alpha(r_0)}{2}\Delta t \simeq 0.812$. However, the apparent horizon is now located at $r_a \simeq 0.92$. So the information at the cutoff will not affect the region beyond the apparent

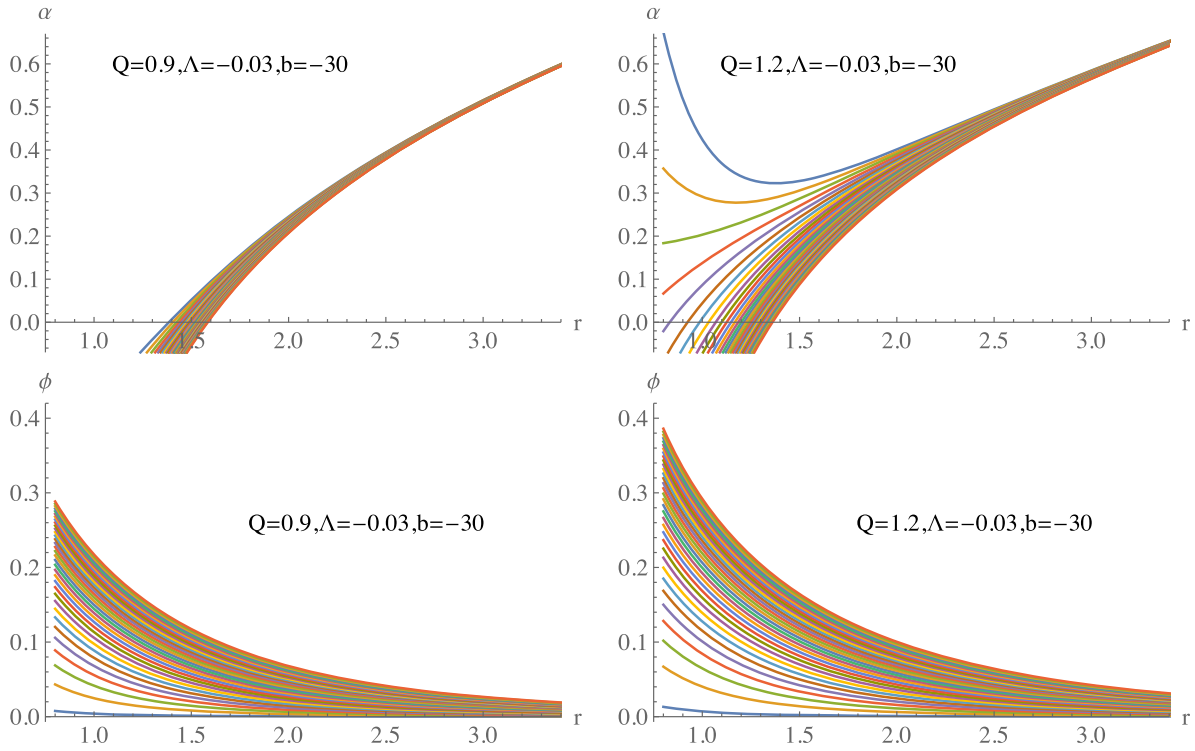

FIG. 1. Sketches of the very early time evolutions (from $t = 0$ to $t = 0.27$) of metric α and scalar ϕ starting from an initial black hole (left panels) or a naked singularity (right panels) spacetime. The blue line corresponds to the initial case. The time step between adjacent lines is $\Delta t \simeq 0.0081$.

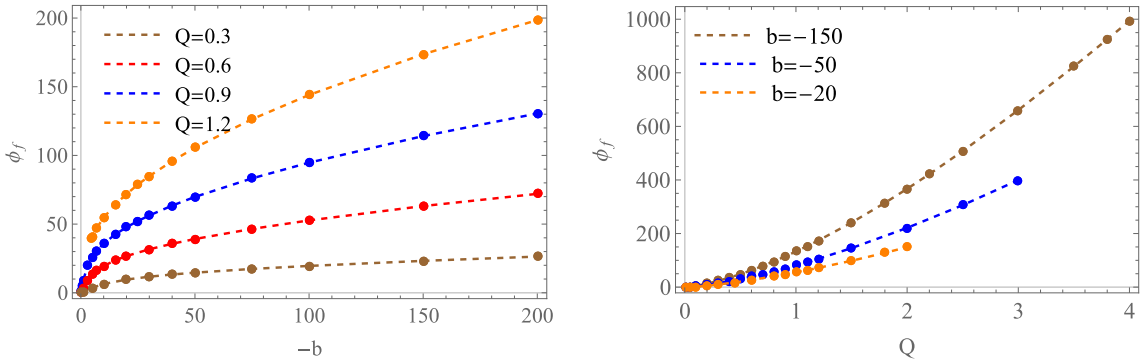

FIG. 2. The final value ϕ_f of ϕ_3 for various b when Q is fixed (left panel), and for various Q when b is fixed (right panel). Note that in the left panel, regular hairy black hole solutions from the evolution of initial naked RN-AdS-like singularity spacetimes exist for $-b > 4.5$ when $Q = 1.2$. In the right panel regular hairy black holes exist for $Q < 2$, 3, 4 when $-b = 20$, 50, 150, respectively. Here $\Lambda = -0.03$.

horizon when a black hole forms. We indeed obtain a stable numerical simulation. A scalarized black hole with $Q > Q_e$ forms at the end.

A. Effects of coupling parameter b on the dynamical scalarisation

In this subsection, we fix $\Lambda = 0.03$ and choose certain Q to study the effects of coupling parameter b on the dynamical scalarization. Since ϕ_3 can be viewed as an indicator of the scalar hair, we show the final value ϕ_f of ϕ_3 in the left panel of Fig. 2. The ϕ_f increases with both $-b$ and Q. Unlike the case in the EMS model where the static hairy black hole solution exists only when $-b$ and Q are large enough [77], there is always a static hairy black hole solution here when $Q < Q_e$. This is reasonable since only a hairy black hole solution exists in EMD theory. The initial RN-AdS black hole solution is dressed with scalar hair soon after the evolution. As the nonminimal coupling between the scalar field and the Maxwell field becomes stronger, the black hole will be dressed heavier. When $Q > Q_e$, our numerical codes work well only if $-b$ is large. This implies that the weak nonminimal coupling between the scalar field and the Maxwell field cannot destroy the original naked RN-AdS-like singularity. Only when the coupling is strong enough would the original naked singularity be destroyed, and the hairy black hole solution gradually develops.

We show the Misner-Sharp mass and the scalar profile at late equilibrium time in the upper panels of Fig. 3. The Misner-Sharp mass tends to the ADM mass $M = 1$ as the radius tends to infinity. For small values of $-b$, the distribution of M_{MS} is close to that of the corresponding RN-AdS black hole. For large values of $-b$, M_{MS} is constant to a relatively large radial distance. At a larger radius, the radial dependence arises due to the presence of the scalar fields. We show the rescaled scalar field $r^2\phi$ which resembles the energy of the scalar in the spherical shell in the lower panels of Fig. 3. The peak moves farther away from the black hole[1] for larger $-b$. In order to better understand the move of peak with $-b$, we can consider the behavior of scalar field perturbation at a certain fixed $-b$ and analyze the potential felt by the scalar field perturbation. Specifically, it can be seen from Eq. (3) that the scalar field perturbation satisfies

$$\nabla^\mu \nabla_\mu \delta\phi = V\delta\phi, \tag{25}$$

with the effective potential $V \equiv b^2 e^{-b\phi} F^{\mu\nu} F_{\mu\nu}$. Since ϕ decreases along the r direction, $e^{-b\phi}$ will be a rapidly decreasing function along r, forming a steep potential near the horizon. When increasing $-b$, the effective potential becomes steeper and drives the peak of $r^2\delta\phi$ away from the horizon. Combining our analysis for Fig. 1, we conclude that the nonminimal coupling between the scalar and the Maxwell field plays two competing roles. On the one hand, it transfers the energy of the Maxwell field to the scalar. The scalar grows and is trapped by the black hole. On the other hand, it behaves as an effective repulsive force that drives the scalar away from the black hole. This is clear when one compares the left panel of Fig. 2 and bottom panels of Fig. 3. The ϕ_f at infinity increases monotonically with $-b$, indicating that more energy is transferred to the scalar. But the scalar value at the black hole horizon increases at first and then decreases with $-b$ due to the repulsive effect of the nonminimal coupling.

Now we show the evolution of $\ln|\phi_3 - \phi_f|$ in the upper panels of Fig. 4. It resembles the behavior of quasinormal mode. The early time behavior of ϕ_3 is closely related to the initial perturbation. Then it oscillates with damping amplitude and converges to the final value ϕ_f. Using the Prony method [81], we worked out the complex frequencies of the dominant damping modes shown in the lower panels of Fig. 4. The imaginary part ω_I increases at first and then decreases with $-b$, indicating that the black hole with

[1]Note that the scalar ϕ itself decreases with r monotonically.

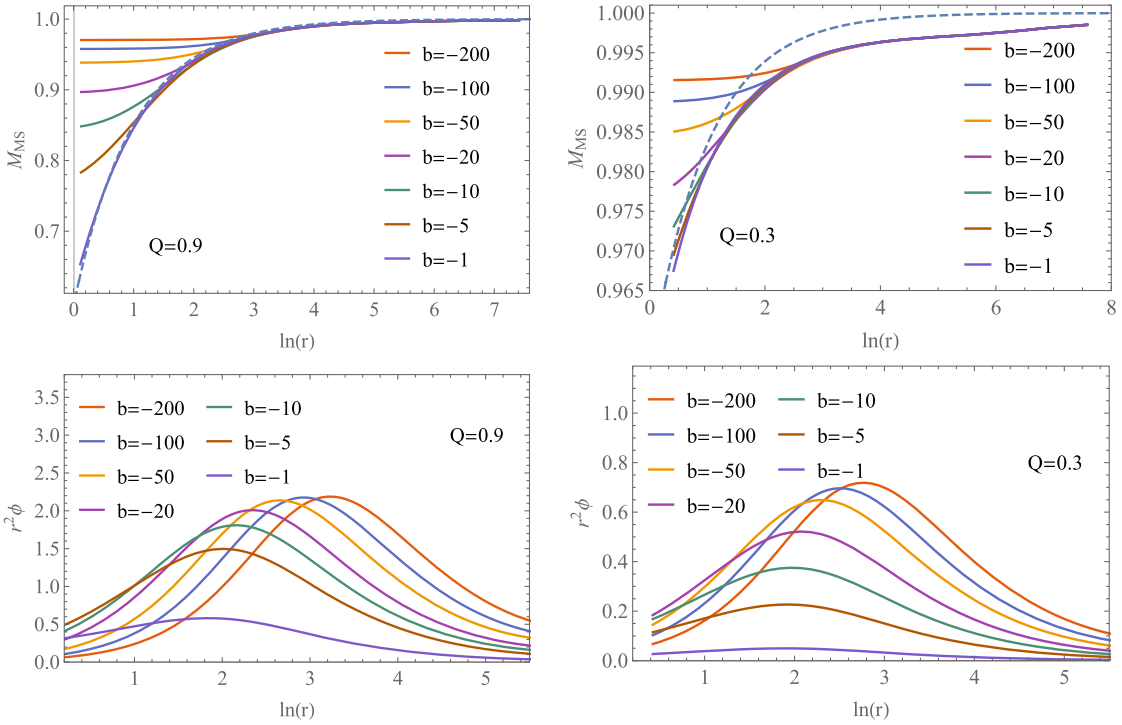

FIG. 3. The Misner-Sharp mass (upper panels) and rescaled scalar profile $r^2\phi$ (lower panels) of the final hairy black holes when $Q = 0.9$ (left panels) and 0.3 (right panels) for various b. The dashed lines in the upper panels correspond to the Misner-Sharp mass of the RN-AdS black hole with $Q = 0.9$ and $Q = 0.3$, respectively. Here $\Lambda = -0.03$.

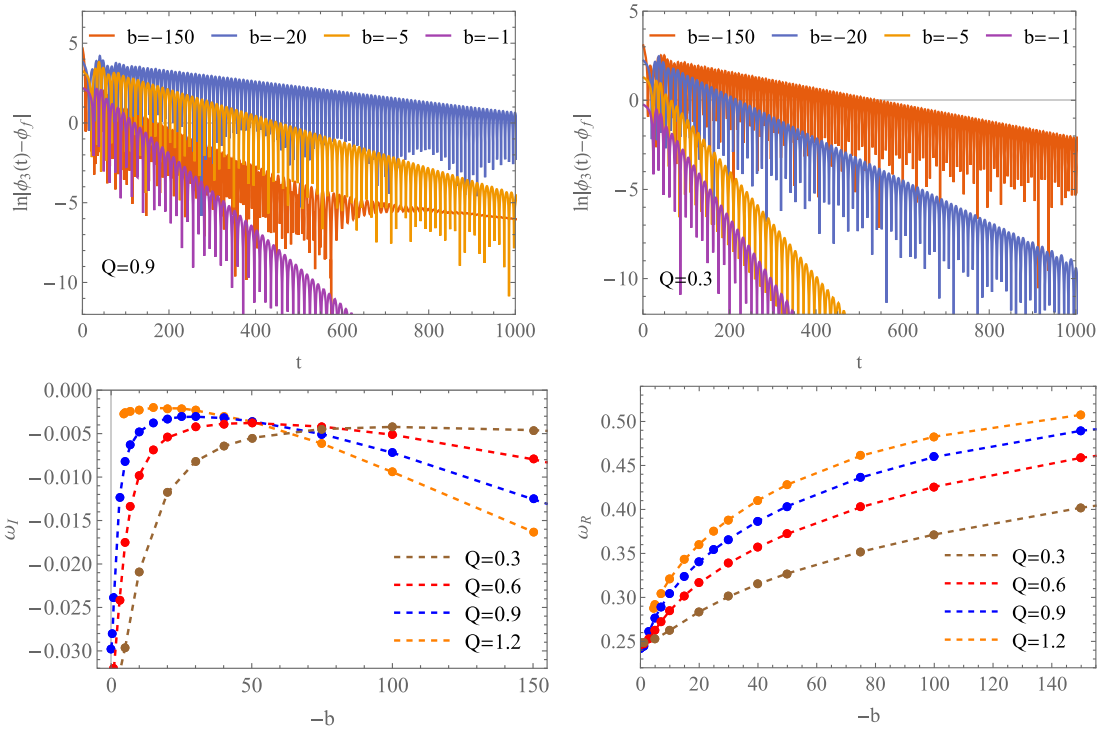

FIG. 4. The evolution of ϕ_3 (upper panels) and the dominant damping modes of ϕ_3 vs b (lower panels). Here $\Lambda = -0.03$.

intermediate nonminimal coupling needs more time to settle down. This can be explained by the two competing roles $-b$ plays. When $-b$ is small, the energy is transferred from the Maxwell field to the scalar. The scalar is caught by the black hole and the initial RN-AdS black hole is destroyed, gradually developing into a hairy black hole solution. But now, the repulsive effect is weak such that the system takes a shorter time to settle down. As $-b$ increases, the initial RN-AdS black hole is also destroyed, but the repulsive effect becomes strong. The competition between the gravitational attraction and the repulsive effect makes the system needs more time to settle down. As $-b$ increases further, the repulsive effect dominates and makes the system settles down more easily. The real part ω_R increases monotonically with $-b$, indicating that the energy transfers faster to the scalar with stronger nonminimal coupling.

To more vividly demonstrate how each component mode evolves, we show the evolution of the amplitudes of each component mode in Fig. 5. These are calculated by partitioning the time axis into many overlapping subintervals with an appropriate offset and performing discrete Fourier transformation on each of these subintervals [82]. We see that all modes decay at late times except the zero mode. The oscillating frequency and decaying rate of the dominant decaying mode are consistent with the ω_R and ω_I from the Prony method. From left to right in Fig. 5 are cases for $-b = 1, 30, 200$, respectively. The real part of the frequency of the dominant decaying mode increases for larger $-b$ and the energy of the scalar increases faster as $-b$ increases. This is consistent with our analysis for the bottom right panel of Fig. 4. We also find that the dominant decaying mode takes a longer time to decay at the intermediate value of $-b$. This is in accordance with the convex behavior of ω_I with $-b$.

Now, we study the evolution of the irreducible mass of the black hole, which is shown in Fig. 6. At early times, the irreducible mass increases abruptly. This is different from the case in the EMS model where the irreducible mass changes little at early times [77]. The RN-AdS black hole solves the EMS theory, the instability of this solution

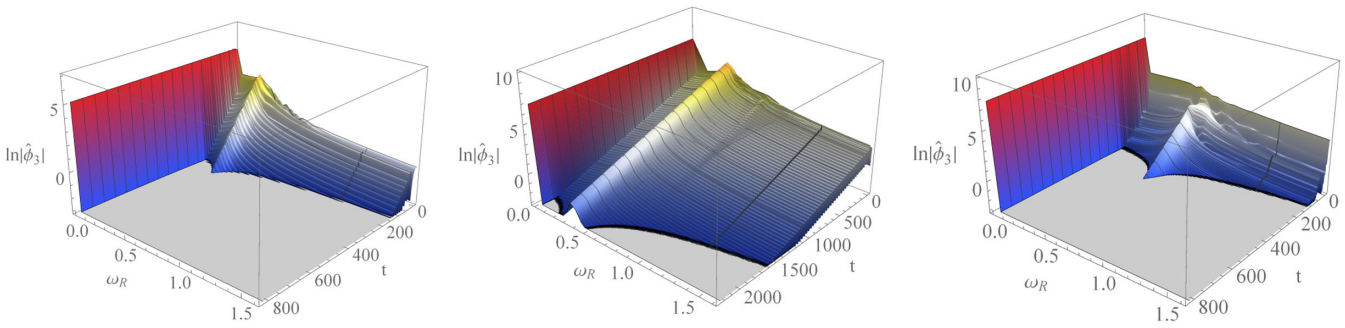

FIG. 5. The evolution of the logarithm of amplitude $\ln|\hat{\phi}_3(t)|$ of discrete Fourier transformation of $\phi_3(t)$ for $b = -1$ (left panel), $b = -30$ (middle panel), and $b = -200$ (right panel) when $Q = 0.9$. Here $\Lambda = -0.03$.

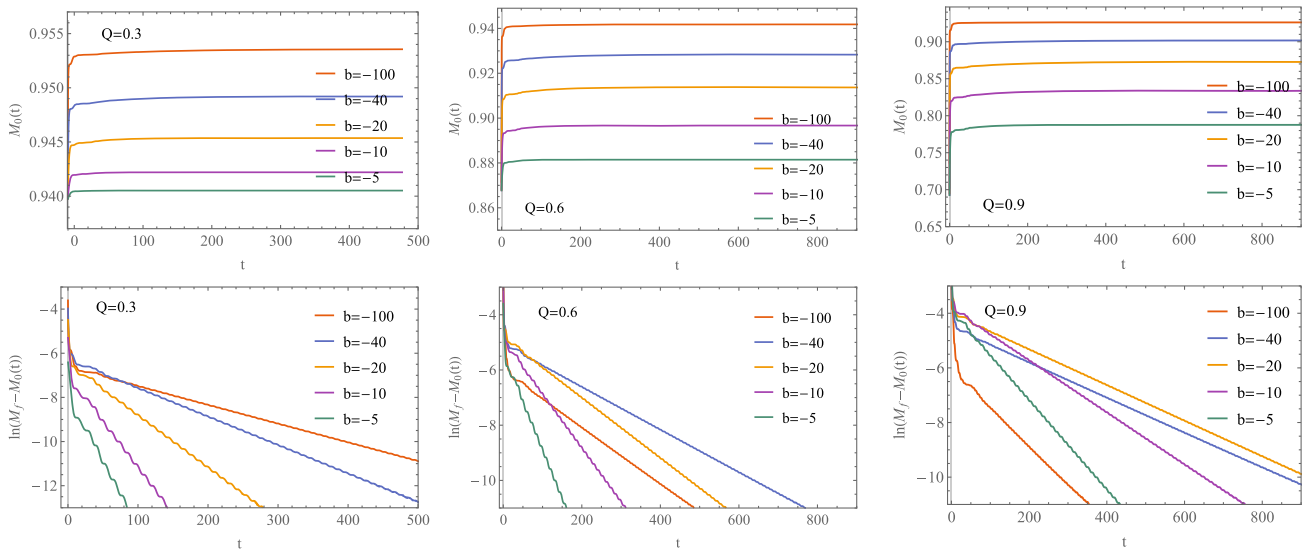

FIG. 6. The evolution of irreducible mass M_0 (upper panels) and $\ln(M_f - M_0)$ (lower panels) of the black hole for various b when $Q = 0.3$, 0.6, and 0.9. Here M_f is the final value of the irreducible mass of the black hole. Here $\Lambda = -0.03$.

triggered by the scalar field is local and it costs time for the scalar perturbation traveling from the initial position to the horizon. Only when the scalar perturbation arrives at the horizon does the black hole begin to grow. However, for the EMD theory, the RN-AdS black hole metric does not solve the model, from the very beginning of the process of evolution the energy outside the horizon is redistributed everywhere, and some of it is swallowed by the central black hole.

At late times, the irreducible mass saturates to the final value M_f with behavior

$$M_0(t) \simeq M_f - e^{-\gamma_f t + c_f}. \tag{26}$$

This is similar to the case in the EMS model at late times. γ_f is the saturating rate and depends on $-b$. Note that the irreducible mass does not decrease here. The increment of the black hole irreducible mass $M_f - M_i$ is shown in the left panel of Fig. 7. Here M_i is the initial irreducible mass of the black hole. When Q is small, $M_f - M_i$ increases monotonically as a function of $-b$. When Q becomes large, $M_f - M_i$ is no longer a monotonic increasing function of $-b$. Instead, it increases at first and then decreases as $-b$ increases. For the model with a large Q, the strength of the effective repulsive force from the Maxwell field affecting the scalar field increase fast and balance the black hole's attractive force thus suppressing the energy flux from outside to inside of the horizon.

The saturating rate γ_f is shown in Fig. 7. When Q is small, γ_f decreases almost monotonically with $-b$. When Q is large, γ_f decreases at first and then increases with $-b$. The irreducible mass saturates faster when $-b$ is small or large enough. This is consistent with Fig. 4. An interesting fact we find is that at late times, there is

$$\gamma_f = -2\omega_I, \tag{27}$$

which can be obtained by comparing the γ_f in Fig. 7 and ω_I in Fig. 4. In fact, the irreducible mass is nothing but the value of ζ at the horizon. Hence the late time evolution of the irreducible mass can be deduced from the evolution of ζ. It is known that the perturbation of the scalar field invokes the backreaction of the metric only at the second order [83]. Namely, there is

$$\delta\zeta \sim (\delta\phi)^2 + \cdots, \tag{28}$$

where "$\cdots$" represents other possible perturbations. Therefore, the saturating rate $-\gamma_f$ of the $\delta\zeta$ should be twice that of ω_I. This relation holds also in the EMS theory [77].

B. Effects of charge Q on the dynamic scalarization

In this subsection, we fix $\Lambda = 0.03$ and choose certain b to study the effects of charge Q on the dynamic scalarization. The final value ϕ_f of ϕ_3 is shown in the right panel of Fig. 2. There is always a hairy black hole solution when Q is nonvanishing. The scalar hair increases monotonically with both Q and $-b$. Note that our numerical evolution codes crash for $Q > 2$, 3, 4 when $-b = 20$, 50, 150, respectively. This implies that the charge to mass ratio of the regular hairy black hole solution cannot be too large [65].

The evolution of ϕ_3 still resembles the behavior of the quasinormal mode. All the modes damp exponentially except the zero modes. The frequencies of the dominant modes are shown in Fig. 8. The real part increases monotonically with Q and $-b$. The imaginary part increases monotonically with Q only when $-b$ is small. For large $-b$, it increases with small Q at first, then it decreases with intermediate Q, and then increases with large Q. In fact, when $-b$ is fixed, the strength of the nonminimal coupling is controlled by charge. When Q is small, the energy of the Maxwell field is transferred to the scalar but the repulsive effect is small, resulting in a hairy black hole solution in a relatively short time. As Q increases, the repulsive effects of the nonminimal coupling become stronger and its competition between the gravitational attraction makes the system need more time to settle down.

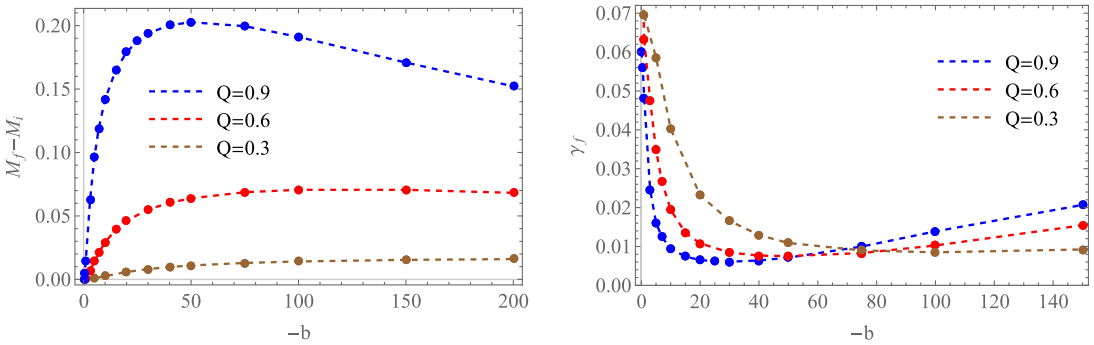

FIG. 7. The increment of the black hole irreducible mass $M_f - M_i$ (left panel) and saturating rate γ_f (right panel) for various b when Q is fixed. Here $\Lambda = -0.03$.

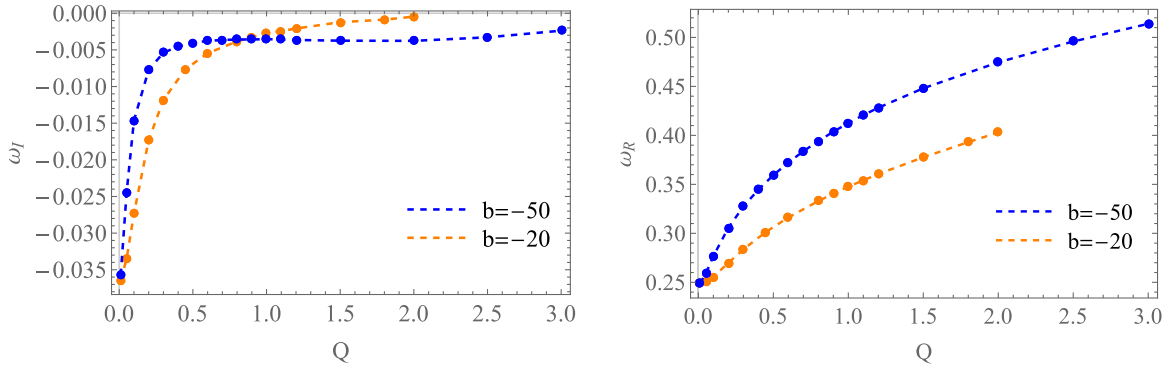

FIG. 8. The imaginary and real part of the frequencies of the dominant damping modes of ϕ_3 vs Q when $b = -150, -50$, and -20. Here $\Lambda = -0.03$.

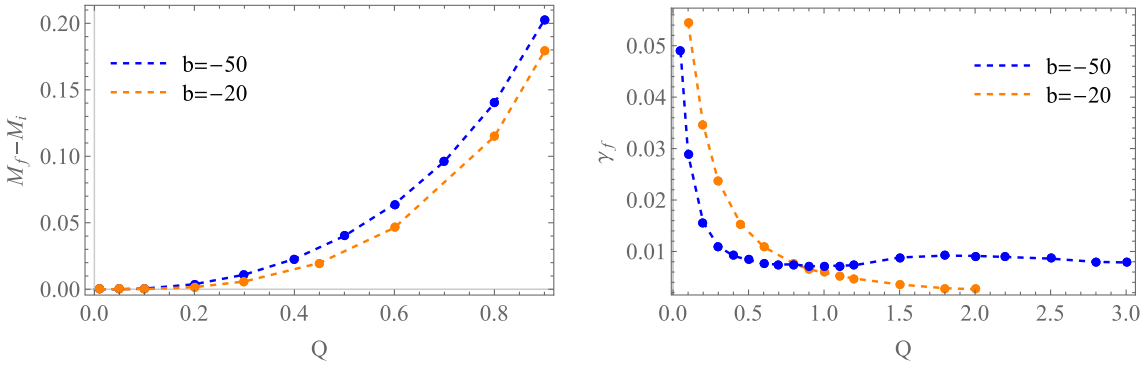

FIG. 9. The increment of irreducible mass of the black hole and the saturating rate for various Q when $b = -50$ and -20. Here $\Lambda = -0.03$.

The irreducible mass M_0 of the black hole still increases abruptly at early times, and then saturates to the final value exponentially. The left panel of Fig. 9 shows[2] that the increment of the irreducible mass $M_f - M_i$ increases monotonically with Q. The right panel shows that the rate γ_f decreases with Q when $-b$ is small. For large $-b$, the rate decreases with small Q at first and then increases with intermediate Q and then decreases again with large Q when $-b$ is large. When the coupling parameter $-b$ is small, it takes a shorter time to settle down for systems with small Q. This is consistent with the results from the imaginary part of the frequencies of the dominant modes in the left panel of Fig. 8 and there is still $\gamma_f = -2\omega_I$ at late times.

C. Effects of the cosmological constant Λ on the black hole evolution

In this subsection, we fix $Q = 0.6$ and choose $b = -20$ and -150 to study the effects of Λ on the black hole evolution. The AdS space looks like a potential well. The larger the $-\Lambda$ is, the deeper and narrower the potential well. Less energy of the Maxwell field is transferred to the scalar field. So the final value ϕ_f decreases with $-\Lambda$ in the left panel of Fig. 10. On the other hand, we find that the final value $\phi_f \propto \Lambda^{-1}$ as $\Lambda \to 0$. This implies that the asymptotic solution in AdS spacetime cannot be generalized straightforwardly to the asymptotic flat spacetime. In fact, the asymptotic expansion of the scalar field behaves as $\phi \sim c + \phi_1/r + \mathcal{O}(r^{-2})$ in asymptotic flat spacetime. The boundary condition should be changed to do the numerical calculations in asymptotic flat spacetime.

The complex frequencies of the dominant damping modes of ϕ_3 are shown in the middle and right panels of Fig. 10. Both the imaginary part of the frequency ω_I and the real part ω_R tend to zero as $\Lambda \to 0$. In AdS space, the smaller the cosmological constant, the flatter the potential well and the smaller the oscillating frequency of the scalar. The scalar needs more time to traverse the space and the system needs much more time to settle down when $-\Lambda$ is very small. As $-\Lambda$ increases, ω_I decreases and ω_R increases. The system oscillates faster and damps faster. Note that unlike the case for the EMS model, there is always a hairy black hole solution for large $-\Lambda$.

[2]We only show the increment when $Q < 1$ since when $Q > 1$, the initial configuration is a naked singularity and there is no corresponding M_i.

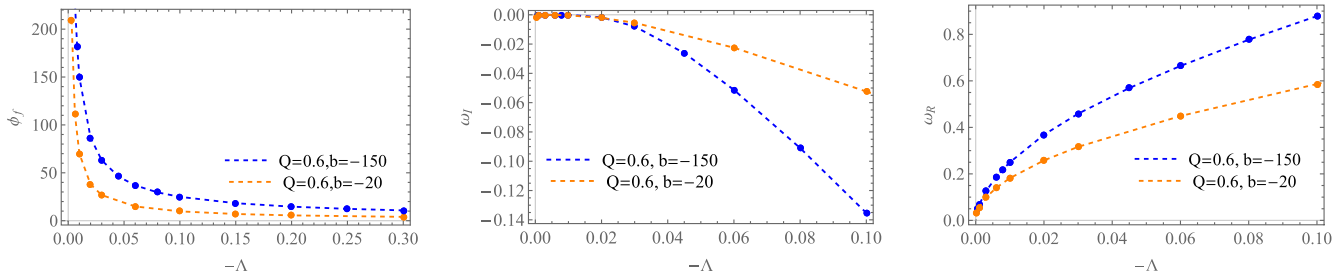

FIG. 10. The behavior of ϕ_f (left), the imaginary part (middle), and the real part (right) of the dominant damping modes of ϕ_3 along the parameter $-\Lambda$.

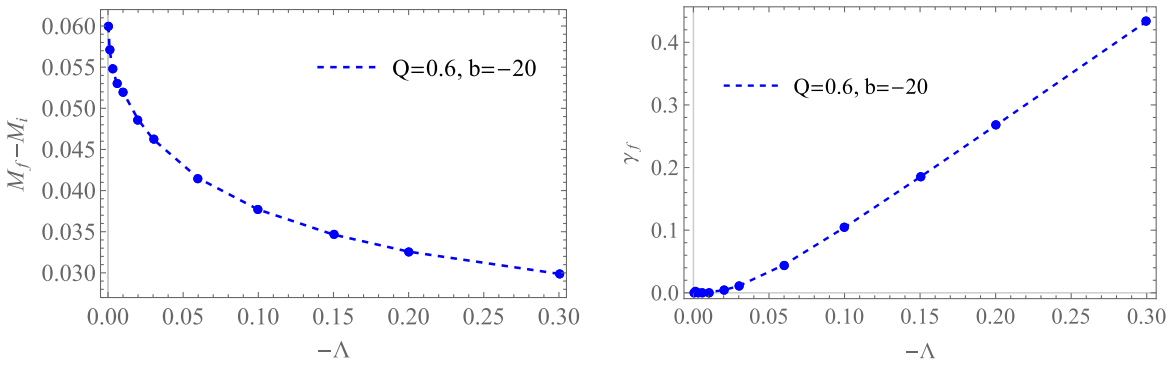

FIG. 11. The increment of the irreducible mass $M_f - M_i$ (left), and the growth rates γ_f for various Λ when $Q = 0.6, b = -20$.

The increment of the irreducible mass of the black hole is shown in the left panel of Fig. 11. At initial times, M_0 increases abruptly and then increases as Eq. (26) at late times. The increment of the irreducible mass is larger for smaller $-\Lambda$, due to the relatively flat potential well which can accumulate more energy of the scalar that draws from the Maxwell field. The saturating rate γ_f of the irreducible mass increases as $-\Lambda$ increases. This means that the system settles down faster as $-\Lambda$ increases.

IV. SUMMARY AND DISCUSSION

We studied the fully nonlinear evolution of the spherical symmetric black holes under a small neutral scalar field perturbation in EMD theory. The equation of motion of the gauge field has no source and can be worked out directly. The free parameters are the black hole charge Q, the cosmological constant Λ, the coupling parameter $-b$, and the ADM mass of the system. The scalar hair can be represented by the coefficient ϕ_3 of order $O(r^{-3})$ in the expansion near infinity, which is determined by the evolution. We fixed the ADM mass $M = 1$ to implement the dimension-lessness of the physical quantities.

We first studied the distribution of Misner-Sharp mass at late equilibrium time. It is constant to a relatively large radial distance, indicating that the scalar hair lies far away from the black hole for large coupling parameters. Then we show the final value of ϕ_3. It increases monotonically with both the black hole charge and the coupling parameter. Unlike the case in the EMS model where the static hairy black hole solution exists only when $-b$ and Q are large enough, there is always a static hairy black hole solution here. The evolution of ϕ_3 resembles the quasinormal mode. The early time behavior of ϕ_3 is closely related to the initial perturbation. Then it oscillates with damping amplitude and converges to the final value. The decaying rate of the dominant decaying mode increases at first and then decreases with $-b$. The irreducible mass of the black hole increases abruptly at initial times and then saturates to the final value exponentially. The saturating rate at late times is twice the decaying rate of the dominant mode of ϕ_3. The system needs more time to settle down when $-b$ is intermediate. Note that we also simulated the evolution of singularity spacetōīime with a large charge to mass ratio. A horizon forms soon and hides the singularity, leaving a regular spacetime geometry outside the horizon.

We also studied the effects of the cosmological constant Λ on evolution. As $\Lambda \to 0$, the final value of ϕ_3 is proportional to Λ^{-1}. The boundary condition should be changed when one implements a numerical simulation in asymptotic flat spacetime. As $\Lambda \to 0$, both the complex frequency of the dominant mode and the saturating rate of

the irreducible mass tend to zero. The system needs much more time to settle down for a small cosmological constant.

A natural generalization of this work is to study the evolution of black holes in asymptotic flat and dS spacetime. The boundary condition is different in that there is not an effective potential barrier at infinity that could bounce the matter back to the bulk [84,85]. Another interesting problem is to study the gravitational collapse or evolution of the black hole with a complex scalar field. The dynamics would be more rich and interesting [80,82,86–88].

ACKNOWLEDGMENTS

P. L. would like to thank Yun-Ha Zha for her kind encouragement during this work. The authors thank De-chang Dai for his helpful discussion. This research is supported by the National Key R&D Program of China under Grant No. 2020YFC2201400, the Guangdong Basic and Applied Basic Research Foundation (Grant No. 2021A1515012374), and the Natural Science Foundation of China under Grants No. 11690021, No. 11947067, No. 12005077, No. 11847055, No. 11905083, and No. 11805083. B. W. was partially supported by NNSF of China under Grant No. 12075202.

[1] W. Israel, Event horizons in static vacuum space-times, Phys. Rev. **164**, 1776 (1967).
[2] B. Carter, Axisymmetric Black Hole Has Only Two Degrees of Freedom, Phys. Rev. Lett. **26**, 331 (1971).
[3] R. Ruffini and J. A. Wheeler, Introducing the black hole, Phys. Today **24**, 30 (1971).
[4] J. D. Bekenstein, Novel "no-scalar-hair" theorem for black holes, Phys. Rev. D **51**, R6608 (1995).
[5] T. P. Sotiriou and V. Faraoni, Black Holes in Scalar-Tensor Gravity, Phys. Rev. Lett. **108**, 081103 (2012).
[6] L. Hui and A. Nicolis, No-Hair Theorem for the Galileon, Phys. Rev. Lett. **110**, 241104 (2013).
[7] T. Ikeda, T. Nakamura, and M. Minamitsuji, Spontaneous scalarization of charged black holes in the scalar-vector-tensor theory, Phys. Rev. D **100**, 104014 (2019).
[8] T. Torii, H. Yajima, and K. i. Maeda, Dilatonic black holes with Gauss-Bonnet term, Phys. Rev. D **55**, 739 (1997).
[9] P. Kanti and K. Tamvakis, Colored black holes in higher curvature string gravity, Phys. Lett. B **392**, 30 (1997).
[10] Z. K. Guo, N. Ohta, and T. Torii, Black holes in the dilatonic Einstein-Gauss-Bonnet theory in various dimensions. I. Asymptotically flat black holes, Prog. Theor. Phys. **120**, 581 (2008).
[11] K. i. Maeda, N. Ohta, and Y. Sasagawa, Black hole solutions in string theory with Gauss-Bonnet curvature correction, Phys. Rev. D **80**, 104032 (2009).
[12] N. Ohta and T. Torii, Global structure of black holes in string theory with Gauss-Bonnet correction in various dimensions, Prog. Theor. Phys. **124**, 207 (2010).
[13] B. Kleihaus, J. Kunz, and E. Radu, Rotating Black Holes in Dilatonic Einstein-Gauss-Bonnet Theory, Phys. Rev. Lett. **106**, 151104 (2011).
[14] B. Kleihaus, J. Kunz, S. Mojica, and E. Radu, Spinning black holes in Einstein-Gauss-Bonnet-dilaton theory: Nonperturbative solutions, Phys. Rev. D **93**, 044047 (2016).
[15] P. Pani, C. F. B. Macedo, L. C. B. Crispino, and V. Cardoso, Slowly rotating black holes in alternative theories of gravity, Phys. Rev. D **84**, 087501 (2011).
[16] P. Pani, E. Berti, V. Cardoso, and J. Read, Compact stars in alternative theories of gravity: Einstein-Dilaton-Gauss-Bonnet gravity, Phys. Rev. D **84**, 104035 (2011).
[17] C. A. R. Herdeiro and E. Radu, Kerr Black Holes with Scalar Hair, Phys. Rev. Lett. **112**, 221101 (2014).
[18] D. Ayzenberg and N. Yunes, Slowly-rotating black holes in Einstein-Dilaton-Gauss-Bonnet gravity: Quadratic order in spin solutions, Phys. Rev. D **90**, 044066 (2014); **91**, 069905 (E) (2015).
[19] E. Babichev and C. Charmousis, Dressing a black hole with a time-dependent Galileon, J. High Energy Phys. 08 (2014) 106.
[20] T. P. Sotiriou and S. Y. Zhou, Black hole hair in generalized scalar-tensor gravity: An explicit example, Phys. Rev. D **90**, 124063 (2014).
[21] R. Benkel, T. P. Sotiriou, and H. Witek, Black hole hair formation in shift-symmetric generalised scalar-tensor gravity, Classical Quantum Gravity **34**, 064001 (2017).
[22] M. S. Volkov and D. V. Galtsov, Non-Abelian Einstein Yang-Mills black holes, JETP Lett. **50**, 346 (1989).
[23] P. Bizon, Colored Black Holes, Phys. Rev. Lett. **64**, 2844 (1990).
[24] B. R. Greene, S. D. Mathur, and C. M. O'Neill, Eluding the no hair conjecture: Black holes in spontaneously broken gauge theories, Phys. Rev. D **47**, 2242 (1993).
[25] K. I. Maeda, T. Tachizawa, T. Torii, and T. Maki, Stability of Non-Abelian Black Holes and Catastrophe Theory, Phys. Rev. Lett. **72**, 450 (1994).
[26] H. Luckock and I. Moss, Black holes have skyrmion hair, Phys. Lett. B **176**, 341 (1986).
[27] S. Droz, M. Heusler, and N. Straumann, New black hole solutions with hair, Phys. Lett. B **268**, 371 (1991).
[28] J. D. Bekenstein, Exact solutions of Einstein conformal scalar equations, Ann. Phys. (N.Y.) **82**, 535 (1974).
[29] T. Damour and G. Esposito-Farese, Nonperturbative Strong Field Effects in Tensor-Scalar Theories of Gravitation, Phys. Rev. Lett. **70**, 2220 (1993).
[30] V. Cardoso, I. P. Carucci, P. Pani, and T. P. Sotiriou, Matter around Kerr black holes in scalar-tensor theories: Scalarization and superradiant instability, Phys. Rev. D **88**, 044056 (2013).
[31] V. Cardoso, I. P. Carucci, P. Pani, and T. P. Sotiriou, Black Holes with Surrounding Matter in Scalar-Tensor Theories, Phys. Rev. Lett. **111**, 111101 (2013).

[32] C. Y. Zhang, S. J. Zhang, and B. Wang, Superradiant instability of Kerr–de Sitter black holes in scalar-tensor theory, J. High Energy Phys. 08 (2014) 011.
[33] T. Harada, Stability analysis of spherically symmetric star in scalar-tensor theories of gravity, Prog. Theor. Phys. **98**, 359 (1997).
[34] C. A. R. Herdeiro and E. Radu, Black hole scalarization from the breakdown of scale invariance, Phys. Rev. D **99**, 084039 (2019).
[35] D. D. Doneva and S. S. Yazadjiev, New Gauss-Bonnet Black Holes with Curvature-Induced Scalarization in Extended Scalar-Tensor Theories, Phys. Rev. Lett. **120**, 131103 (2018).
[36] H. O. Silva, J. Sakstein, L. Gualtieri, T. P. Sotiriou, and E. Berti, Spontaneous Scalarization of Black Holes and Compact Stars from a Gauss-Bonnet Coupling, Phys. Rev. Lett. **120**, 131104 (2018).
[37] G. Antoniou, A. Bakopoulos, and P. Kanti, Evasion of No-Hair Theorems and Novel Black-Hole Solutions in Gauss-Bonnet Theories, Phys. Rev. Lett. **120**, 131102 (2018).
[38] P. V. Cunha, C. A. Herdeiro, and E. Radu, Spontaneously Scalarized Kerr Black Holes in Extended Scalar-Tensor-Gauss-Bonnet Gravity, Phys. Rev. Lett. **123**, 011101 (2019).
[39] A. Dima, E. Barausse, N. Franchini, and T. P. Sotiriou, Spin-Induced Black Hole Spontaneous Scalarization, Phys. Rev. Lett. **125**, 231101 (2020).
[40] C. A. R. Herdeiro, E. Radu, H. O. Silva, T. P. Sotiriou, and N. Yunes, Spin-Induced Scalarized Black Holes, Phys. Rev. Lett. **126**, 011103 (2021).
[41] E. Berti, L. G. Collodel, B. Kleihaus, and J. Kunz, Spin-Induced Black-Hole Scalarization in Einstein-Scalar-Gauss-Bonnet Theory, Phys. Rev. Lett. **126**, 011104 (2021).
[42] K. Lin, S. Zhang, C. Zhang, X. Zhao, B. Wang, and A. Wang, No static regular black holes in Einstein-complex-scalar-Gauss-Bonnet gravity, Phys. Rev. D **102**, 024034 (2020).
[43] H. Guo, S. Kiorpelidi, X. M. Kuang, E. Papantonopoulos, B. Wang, and J. P. Wu, Spontaneous holographic scalarization of black holes in Einstein-scalar-Gauss-Bonnet theories, Phys. Rev. D **102**, 084029 (2020).
[44] L. G. Collodel, B. Kleihaus, J. Kunz, and E. Berti, Spinning and excited black holes in Einstein-scalar-Gauss-Bonnet theory, Classical Quantum Gravity **37**, 075018 (2020).
[45] D. D. Doneva, S. Kiorpelidi, P. G. Nedkova, E. Papantonopoulos, and S. S. Yazadjiev, Charged Gauss-Bonnet black holes with curvature induced scalarization in the extended scalar-tensor theories, Phys. Rev. D **98**, 104056 (2018).
[46] Y. Brihaye, C. Herdeiro, and E. Radu, The scalarised Schwarzschild-NUT spacetime, Phys. Lett. B **788**, 295 (2019).
[47] C. A. R. Herdeiro, E. Radu, N. Sanchis-Gual, and J. A. Font, Spontaneous Scalarization of Charged Black Holes, Phys. Rev. Lett. **121**, 101102 (2018).
[48] G. Guo, P. Wang, H. Wu, and H. Yang, Scalarized Einstein-Maxwell-scalar black holes in anti–de Sitter spacetime, Eur. Phys. J. C **81**, 864 (2021).
[49] J. L. Blázquez-Salcedo, C. A. R. Herdeiro, J. Kunz, A. M. Pombo, and E. Radu, Einstein-Maxwell-scalar black holes: The hot, the cold and the bald, Phys. Lett. B **806**, 135493 (2020).
[50] C. A. R. Herdeiro, J. M. S. Oliveira, and E. Radu, A class of solitons in Maxwell-scalar and Einstein-Maxwell-scalar models, Eur. Phys. J. C **80**, 23 (2020).
[51] D. Astefanesei, C. Herdeiro, J. Oliveira, and E. Radu, Higher dimensional black hole scalarization, J. High Energy Phys. 09 (2020) 186.
[52] D. Astefanesei, C. Herdeiro, A. Pombo, and E. Radu, Einstein-Maxwell-scalar black holes: Classes of solutions, dyons and extremality, J. High Energy Phys. 10 (2019) 078.
[53] P. G. S. Fernandes, C. A. R. Herdeiro, A. M. Pombo, E. Radu, and N. Sanchis-Gual, Charged black holes with axionic-type couplings: Classes of solutions and dynamical scalarization, Phys. Rev. D **100**, 084045 (2019).
[54] J. M. S. Oliveira and A. M. Pombo, Spontaneous vectorization of electrically charged black holes, Phys. Rev. D **103**, 044004 (2021).
[55] B. P. Abbott *et al.* (LIGO Scientific and Virgo Collaborations), Observation of Gravitational Waves from a Binary Black Hole Merger, Phys. Rev. Lett. **116**, 061102 (2016).
[56] L. Barack *et al.*, Black holes, gravitational waves and fundamental physics: A roadmap, Classical Quantum Gravity **36**, 143001 (2019).
[57] K. Akiyama *et al.* (Event Horizon Telescope Collaboration), First M87 Event Horizon Telescope results. I. The shadow of the supermassive black hole, Astrophys. J. **875**, L1 (2019).
[58] K. Akiyama *et al.* (Event Horizon Telescope Collaboration), First M87 Event Horizon Telescope results. IV. Imaging the central supermassive black hole, Astrophys. J. Lett. **875**, L4 (2019).
[59] K. Akiyama *et al.* (Event Horizon Telescope Collaboration), First M87 Event Horizon Telescope results. VI. The shadow and mass of the central black hole, Astrophys. J. Lett. **875**, L6 (2019).
[60] M. Khodadi, A. Allahyari, S. Vagnozzi, and D. F. Mota, Black holes with scalar hair in light of the Event Horizon Telescope, J. Cosmol. Astropart. Phys. 09 (2020) 026.
[61] A. Rahmani, M. Khodadi, M. Honardoost, and H. R. Sepangi, Instability and no-hair paradigm in *d*-dimensional charged-AdS black holes, Nucl. Phys. **B960**, 115185 (2020).
[62] T. Kaluza, Sitzungsber. Preuss. Akad. Wiss. Berlin (Math. Phys.) **1921**, 966 (1921).
[63] E. Cremmer and B. Julia, Phys. Lett. **80B**, 48 (1978).
[64] G. W. Gibbons and K. i. Maeda, Black holes and membranes in higher dimensional theories with dilaton fields, Nucl. Phys. **B298**, 741 (1988).
[65] D. Garfinkle, G. T. Horowitz, and A. Strominger, Charged black holes in string theory, Phys. Rev. D **43**, 3140 (1991); **45**, 3888(E) (1992).
[66] C. Y. Zhang, S. J. Zhang, and B. Wang, Charged scalar perturbations around Garfinkle-Horowitz-Strominger black holes, Nucl. Phys. **B899**, 37 (2015).
[67] J. L. Ripley and F. Pretorius, Gravitational collapse in Einstein dilaton-Gauss-Bonnet gravity, Classical Quantum Gravity **36**, 134001 (2019).
[68] J. L. Ripley and F. Pretorius, Scalarized black hole dynamics in Einstein-dilaton-Gauss-Bonnet gravity, Phys. Rev. D **101**, 044015 (2020).

[69] J. L. Ripley and F. Pretorius, Dynamics of a $\mathbb{Z}_2$ symmetric EdGB gravity in spherical symmetry, Classical Quantum Gravity **37**, 155003 (2020).
[70] D. D. Doneva and S. S. Yazadjiev, On the dynamics of the nonrotating and rotating black hole scalarization, Phys. Rev. D **103**, 064024 (2021).
[71] H. O. Silva, H. Witek, M. Elley, and N. Yunes, Dynamical Scalarization and Descalarization in Binary Black Hole Mergers, Phys. Rev. Lett. **127**, 031101 (2021).
[72] H. Witek, L. Gualtieri, P. Pani, and T. P. Sotiriou, Black holes and binary mergers in scalar Gauss-Bonnet gravity: Scalar field dynamics, Phys. Rev. D **99**, 064035 (2019).
[73] D. Astefanesei, J. L. Blázquez-Salcedo, C. Herdeiro, E. Radu, and N. Sanchis-Gual, Dynamically and thermodynamically stable black holes in Einstein-Maxwell-dilaton gravity, J. High Energy Phys. 07 (2020) 063.
[74] E. W. Hirschmann, L. Lehner, S. L. Liebling, and C. Palenzuela, Black hole dynamics in Einstein-Maxwell-Dilaton theory, Phys. Rev. D **97**, 064032 (2018).
[75] P. G. S. Fernandes, C. A. R. Herdeiro, A. M. Pombo, E. Radu, and N. Sanchis-Gual, Spontaneous scalarisation of charged black holes: Coupling dependence and dynamical features, Classical Quantum Gravity **36**, 134002 (2019); **37**, 049501(E) (2020).
[76] Y. Brihaye, C. Herdeiro, and E. Radu, Black hole spontaneous scalarisation with a positive cosmological constant, Phys. Lett. B **802**, 135269 (2020).
[77] C. Y. Zhang, P. Liu, Y. Liu, C. Niu, and B. Wang, Dynamical charged black hole spontaneous scalarization in anti–de Sitter spacetimes, Phys. Rev. D **104**, 084089 (2021).
[78] A. Bakopoulos, G. Antoniou, and P. Kanti, Novel black-hole solutions in Einstein-Scalar-Gauss-Bonnet theories with a cosmological constant, Phys. Rev. D **99**, 064003 (2019).
[79] H. Maeda, Exact dynamical AdS black holes and wormholes with a Klein-Gordon field, Phys. Rev. D **86**, 044016 (2012).
[80] P. M. Chesler and L. G. Yaffe, Numerical solution of gravitational dynamics in asymptotically anti–de Sitter spacetimes, J. High Energy Phys. 07 (2014) 086.
[81] E. Berti, V. Cardoso, J. A. Gonzalez, and U. Sperhake, Mining information from binary black hole mergers: A comparison of estimation methods for complex exponentials in noise, Phys. Rev. D **75**, 124017 (2007).
[82] P. Bosch, S. R. Green, and L. Lehner, Nonlinear Evolution and Final Fate of Charged Anti–de Sitter Black Hole Superradiant Instability, Phys. Rev. Lett. **116**, 141102 (2016).
[83] R. Brito, V. Cardoso, and P. Pani, in *Superradiance: New Frontiers in Black Hole Physics*, Lecture Notes in Physics Vol. 906, edited by R. Brito, V. Cardoso, and P. Pani (Springer, New York, 2015).
[84] S. Hod and T. Piran, Critical behavior and universality in gravitational collapse of a charged scalar field, Phys. Rev. D **55**, 3485 (1997).
[85] C. Y. Zhang, S. J. Zhang, D. C. Zou, and B. Wang, Charged scalar gravitational collapse in de Sitter spacetime, Phys. Rev. D **93**, 064036 (2016).
[86] Ó. J. C. Dias and R. Masachs, Hairy black holes and the endpoint of AdS_4 charged superradiance, J. High Energy Phys. 02 (2017) 128.
[87] N. Sanchis-Gual, J. C. Degollado, P. J. Montero, J. A. Font, and C. Herdeiro, Explosion and Final State of an Unstable Reissner-Nordström Black Hole, Phys. Rev. Lett. **116**, 141101 (2016).
[88] P. M. Chesler and D. A. Lowe, Nonlinear Evolution of the AdS_4 Superradiant Instability, Phys. Rev. Lett. **122**, 181101 (2019).